Improving Anytime Prediction with Parallel Cascaded Networks and a Temporal-Difference Loss

Michael L. Iuzzolino
Google Research, Brain Team and
Department of Computer Science, University of Colorado

Michael C. Mozer
Google Research, Brain Team and
Institute of Cognitive Science, University of Colorado

Samy Bengio
Google Research, Brain Team*

Abstract

Although deep feedforward neural networks share some characteristics with the primate visual system, a key distinction is their dynamics. Deep nets typically operate in *serial* stages wherein each layer completes its computation before processing begins in subsequent layers. In contrast, biological systems have *cascaded* dynamics: information propagates from neurons at all layers in parallel but transmission occurs gradually over time, leading to speed-accuracy trade offs even in feedforward architectures. We explore the consequences of biologically inspired parallel hardware by constructing cascaded ResNets in which each residual block has propagation delays but all blocks update in parallel in a stateful manner. Because information transmitted through skip connections avoids delays, the functional depth of the architecture increases over time, yielding anytime predictions that improve with internal-processing time. We introduce a temporal-difference training loss that achieves a strictly superior speed-accuracy profile over standard losses and enables the cascaded architecture to outperform state-of-the-art anytime-prediction methods. The cascaded architecture has intriguing properties, including: it classifies typical instances more rapidly than atypical instances; it is more robust to both persistent and transient noise than is a conventional ResNet; and its time-varying output trace provides a signal that can be exploited to improve information processing and inference.

Since the earliest investigations of artificial neural nets, their design has been informed by biological neural nets [33]. Perhaps the most compelling example is the convolutional net for machine vision, which has adopted properties of primate cortical neuroanatomy including a hierarchical layered organization, local receptive fields, and spatial equivariance [11]. In this article, we investigate computational consequences of two fundamental properties of biological information processing systems that have not been considered in the design of deep neural nets. First, *the brain consists of massively parallel, dedicated hardware with neurons throughout the cortex updating continuously and simultaneously.* Second, *information*

*Currently at Apple.

Preprint. Under review.

transmission between neurons introduces time delays [1]. As a result, unrefined and possibly incomplete neural state in one region is transmitted to the next region even as the state evolves; and even feedforward connectivity yields a speed-accuracy trade off in which the initial response to a static input occurs rapidly but can be inaccurate, with the output gradually improving over internal processing time. Following [32], we refer to such an architecture as *cascaded*.

Cascaded dynamics contrast sharply with the dynamics of standard feedforward nets, which operate in *serial* stages, each layer completing its computation before subsequent layers begin processing. Cascaded dynamics are also quite different than the dynamics of vision models with recurrent connections [e.g., 22, 24, 34, 41], which, given a static input, may iteratively update, but layer updates are still computed serially with each layer completing its computation and then feeding it immediately to the next layer (or back to itself). Fundamentally, our investigation asks: Supposing we take a step toward biological realism with massively parallel hardware and relatively slow inter-neuron communication, what are the computational benefits and consequences?

We construct cascaded networks by introducing propagation delays in deep feedforward nets provided with a static input. We treat the net as massively parallel such that all units across all layers are updated simultaneously and iteratively. We focus on the ResNet architecture [13] and we introduce a propagation delay into each residual block (Figure 1a). Because the skip connection permits faster transmission of more primitive perceptual representations, the functional depth of the resulting architecture increases over internal-processing time, yielding a trade off between processing speed and complexity of processing. Consequently, the architecture offers a natural, integral mechanism for *anytime prediction* [53]. Speed-accuracy trade offs are a fundamental characteristic of human information processing [21, 38] and human perception has been modeled with deep learning anytime prediction methods [26].

Although we focus on the ResNet, our approach can be incorporated into any model with skip connections (e.g., Highway Nets [43], DenseNet [17], U-Net [39], Transformers [47]). The contrast between a *serial*, one-layer-at-a-time model and a *cascaded*, parallel-update model is illustrated in Figures 1b and 1c, respectively. To step through the operation of the cascaded model, at time 1, only the first residual block has received meaningful input, and the model prediction is therefore based only on this block's computation. At time 2, *all* higher residual blocks have received input from block 1, and the output is therefore based on *all* blocks' computations, though blocks 2 and above have deficient input. At each subsequent time, all blocks are receiving meaningful input, but it is not until time t that block t has reached its asymptotic output because its input does not stabilize until $t-1$. In essence, the cascaded model behaves like a WideResNet [51] on the first steps and then becomes a deep ResNet.

Our work makes the following key contributions.

- We demonstrate the superiority of the cascaded architecture to the serial (Figures 1b,c), indicating that parallelism can be exploited in a way that has not previously been studied.
- We propose and evaluate a novel training objective aimed at improving the predictions of anytime models. This *temporal-difference (TD) loss* [44] encourages the most accurate response as quickly as possible. TD training improves the performance of both cascaded and serial architectures. Although a rich literature exists aimed at reducing the number of computational steps required to obtain an accurate answer [2, 3, 4, 5, 10, 14, 15, 16, 18, 19, 23, 28, 34, 36, 40, 46, 49, 52], all of this work uses a degenerate form of TD for training and our results suggest that these models can be improved using TD.
- The cascaded model trained with TD (CascadedTD) tends to respond most rapidly to prototypical exemplars, whereas training with the standard cross-entropy loss (CascadedCE) does not (Figure 2). We assess with three quantitative prototypicality measures, and we further show that CascadedTD rapidly homes in on the correct semantic family, whereas CascadedCE does not. These facts indicate that CascadedTD organizes knowledge differently across layers than does CascadedCE.
- We show that CascadedTD obtains a strictly superior speed-accuracy profile compared to previously proposed anytime prediction models, which are all based on a serial architecture.

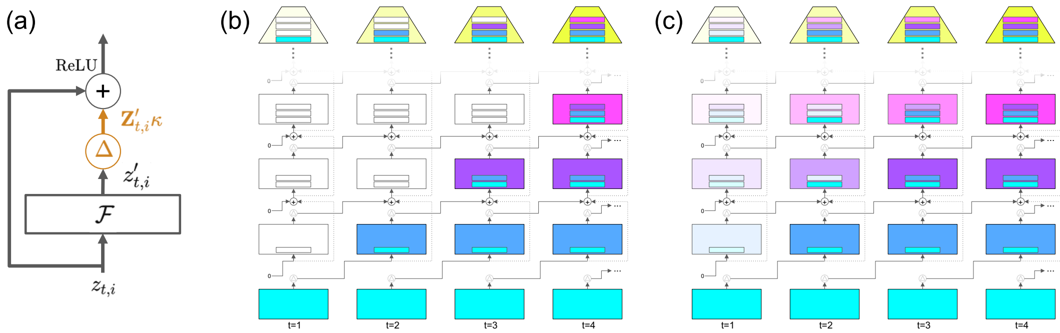

Figure 1: (a) ResNet building block, with additional delay component (Δ, in orange) that convolves a temporal kernel with the block output. Details in text. (b) Unrolling a standard *serial* ResNet in time (columns). Each rectangle is a ResNet block, which may consist of two or more convolutional layers. Blocks are updated sequentially. The color intensity (saturation) of a block indicates the extent to which a block has been completely activated. The narrow bars within each block signify the activation state of all blocks below that are contributing to the block's state (via skip connections). The yellow trapezoid at the top shows the layer information available at each time for classification. (c) Unrolling a *cascaded* ResNet. Note partial activations propagating through architecture due to parallel updates of all layers.

- We demonstrate other virtues of CascadedTD: it is more robust to input noise, and its time-varying output trace provides useful signals for *meta-cognitive* processes—separately trained nets that make judgments about the cascaded architecture's accuracy.

Related Work

Prior research on cascaded models. From a psychological perspective, McClelland [32] characterizes human mental computation in terms of a hierarchy of leaky integrators that continually transmit partial information as it becomes available. We are aware of no work in deep learning on static image processing with cascaded models, but there exist two investigations focused on video sequence processing where the model state from the previous frame is used to efficiently process the next. Fischer et al. [10] present a *streaming rollout* framework for recurrent nets and they very briefly explore the temporal dynamics of cascaded models, showing benefits to early predictions. Carreira et al. [5] present a causal video understanding model that performs depth-parallel computation with the objective of improving video processing efficiency via the maximizing throughput, minimizing latency, and reducing clock cycles.

Recurrent nets for vision. Recurrent nets have been used in vision [e.g., 19, 22, 24, 41, 42], which adds a dimension of internal processing time for every external input (see also [12]). However, these models perform serial layerwise updates and therefore fundamentally differ in their operation from cascaded models.

Anytime prediction. Anytime prediction models [2, 8, 14, 15, 16, 18, 19, 23, 27, 28, 30, 34, 36, 40, 46, 48, 49, 52] assume serial operation of layers but allow for predictions to be made from intermediate layers of the architecture. In the simplest case, after t steps, t layers have been activated, and at each step, a prediction is made from the last activated layer [e.g., 15, 23]. Figure 1b illustrates a serial model that performs anytime prediction. Some of these models have intrinsic stopping criteria [e.g., 6]; others rely on selection of a stopping confidence threshold [e.g., 23, 46, 49].

Temporal-difference learning. TD learning has a rich history, mostly in the RL community for value function estimation. TD learning can be used for supervised training as well, and in fact the two previous works in deep learning using cascaded models [5, 10] perform supervised training to attain the correct model classification at each step. The form of training is equivalent to a degenerate case of temporal difference learning, TD(1), which we show to have inferior performance. A variety of non-cascaded models, both recurrent [19, 34, 52] and feedforward [2, 3, 4, 14, 15, 16, 18, 23, 28, 36, 40, 46, 49], aim to reduce the number of computational steps required to obtain an accurate output. All use TD(1) for

Figure 2: (a) Three CIFAR-100 instances categorized rapidly (left) and slowly (right) by a cascaded model trained using a TD loss. (b) same as (a) for a standard cross-entropy loss. When trained with the TD loss, the cascaded model stratifies instances by typicality, with rapid processing of prototypical views on a homogenenous background and slow processing of unusual and cluttered views.

training. No previous research has explored the general formulation of TD for improving anytime prediction.

Deep Cascaded Networks

Many modern deep architectures—including ResNet [13], Highway Nets [43], DenseNet [17], U-Net [39]—incorporate skip connections that bypass strictly layered feedforward connectivity, analogous to the architecture of visual cortex [9]. Under the biological assumption that signals transmitted through a neural layer are delayed relative to signals that bypass the layer, we construct a cascaded model using ResNets by introducing a novel computational component that delays the transmission of signals from the output of each computational layer, denoted Δ in Figure 1a. Because these delays extend processing in time, the hidden states require a time index. The input to ResNet block i at time t is denoted $\boldsymbol{z}_{t,i}$. The block transforms this input via the residual transform, yielding $\boldsymbol{z}'_{t,i} = \mathcal{F}(\boldsymbol{z}_{t,i})$. We conceive of Δ as a tapped delay-line memory of the transform history, $\boldsymbol{Z}'_{t,i} = [\boldsymbol{z}'_{t,i}\ \boldsymbol{z}'_{t-1,i}\ \ldots\ \boldsymbol{z}'_{1,i}]$, which is convolved with a temporal kernel $\boldsymbol{\kappa}$ to produce the block output

$$\boldsymbol{z}_{t,i+1} = \mathrm{ReLU}\left(\boldsymbol{z}_{t,i} + \boldsymbol{Z}'_{t,i}\boldsymbol{\kappa}\right). \tag{1}$$

The kernel $\boldsymbol{\kappa} = [1\ 0\ 0\ldots 0]$ recovers the standard ResNet in which communication between layers is instantaneous. We consider two kernels to introduce time delays. With $\boldsymbol{\kappa} = [0\ \ 1\ \ 0\ \ 0\ \ \ldots 0]$, a discrete one-step delay is introduced (*OSD* for short). With $\boldsymbol{\kappa} = (1-\alpha)[1\ \ \alpha\ \ \alpha^2\ \ \alpha^3\ldots]$, we obtain exponentially weighted smoothing (*EWS* for short), with larger $\alpha \in [0, 1)$ producing slower transmission times. Note that both of these special kernels have efficient implementations: the OSD kernel with a one-element queue, the EWS kernel with incremental update and a finite (one-step) state vector,

$$\boldsymbol{Z}'_{t,i}\boldsymbol{\kappa} = \alpha\boldsymbol{Z}'_{t-1,i}\boldsymbol{\kappa} + (1-\alpha)\boldsymbol{z}'_{t,i}.$$

We use the OSD kernel for training all models. Modifications of batch norm were required to do time-step-conditional normalization. All experiments use a ResNet-18, which has 8 residual blocks and hence 8 time delays. (We have done experiments with larger ResNets and the additional compute did not affect qualitative properties.) We also add a time delay to the output of the model's first convolutional layer. Consequently, with the OSD kernel, the cascaded model requires 9 updates for the output to reach asymptote. The cascaded and serial models with the same weights will necessarily produce identical asymptotic outputs.

To obtain a finer temporal granularity at evaluation, some simulations switch to the EWS kernel with $\alpha = 0.9$. Temporal dynamics are qualitatively similar for OSD and EWS, but EWS allows us to better distinguish individual examples in terms of their fine-grain timing. EWS with $\alpha = 0.9$ requires about 70 steps for the output to asymptote. The choice of α over a had no impact on our findings, as long as it slowed transmission.

Training Cascaded Networks with TD(λ)

To allow for anytime prediction, we include an output head following each of the T residual blocks in both the serial and cascaded models (see Figure 1b,c, respectively). The output heads may share weights or have separate weights. To encourage correct outputs sooner, we use temporal difference (TD) learning [44] over the output sequence. Readers may associate TD methods with reinforcement learning because TD methods have traditionally been used to predict future rewards. However, TD methods are fundamentally designed for

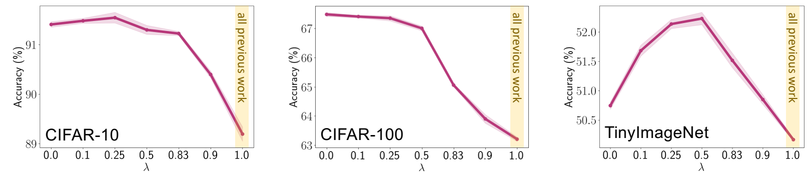

Figure 3: Effect of TD hyperparameter λ on CascadedTD test accuracy for three data sets. $\lambda = 1$ corresponds to the training methodology of all past research on anytime prediction, which is inferior to any $\lambda < 1$ for all data sets. Shaded error bands—hard to see on most curves—indicate ± 1 SEM, corrected to remove performance variance due to weight initialization and unrelated to λ [31].

supervised learning. We use TD to predict a future outcome—the correct classification of an image—from a sequence of successively more informative states—the information flowing through the ResNet at each internal time step.

TD(λ) specifies a target output y_t at each time $t \in \{1, ...T\}$ based on the model's actual output $\hat{y}_{t+i}$ at future times $t+i$ for $i > 0$, and the eventual outcome or true target, y_{true}:

$$y_t = (1-\lambda)\left[\sum_{i=1}^{T-t} \lambda^{i-1} \hat{y}_{t+i}\right] + \lambda^{T-t} y_{\text{true}}, \tag{2}$$

where $\lambda \in [0, 1]$ is a free parameter that essentially specifies the time horizon for prediction. TD(1) predicts the eventual outcome at each step; TD(0) predicts the model's output at the next step (and the eventual outcome at the final step). Given target y_t and actual output $\hat{y}_t$, we specify a cross-entropy loss, $\mathcal{L} = \sum_{t=0}^{T} H(y_t, \hat{y}_t)$, where $H(p, q)$ is the cross-entropy. Note that y_t must be treated as a constant, not as a differentiable variable, via a `stop_gradient` (for TensorFlow or Jax) or `requires_grad=False` (for PyTorch). Although Equation 2 requires knowledge of all subsequent network states, the beauty of TD methods is that this loss can be computed incrementally (see Appendix). The edge cases TD(0) and TD(1) have particularly trivial implementations. Past research has always used TD(1) for specifying intermediate targets, but we will show that TD(1) is suboptimal because the model is penalized for being unable to classify correctly at the earliest steps.

Results

TD(λ) Training

We conducted a sweep over hyperparameter λ to determine its effect on asymptotic accuracy of CascadedTD. Figure 3 shows results from five replications of CascadedTD on CIFAR-100, CIFAR-10, and TinyImageNet. The hyperparameter has a systematic effect, consistent with classic studies with linear models [45, Chapter 12]. Importantly, $\lambda = 1$, which is the implicit choice of *every* previous anytime-prediction model [2, 8, 14, 15, 16, 18, 19, 23, 27, 28, 30, 34, 36, 40, 46, 48, 49, 52], obtains the poorest performance for all three data sets, significantly worse than $\lambda \approx .5$. The essential explanation is that larger λ penalize the network for behavior it does not have the capability to achieve: obtaining the asymptotic prediction at the earliest time steps. To paraphrase the classic illustration of TD from Sutton [44], if the task is predicting the weather on December 31, no model can predict as accurately on December 1 as on December 30. Selecting $\lambda < 1$ shortens the prediction horizon; $\lambda = 0$ corresponds with requiring a prediction only of the weather on the next day.

In the rest of the article, we report results for CascadedTD with $\lambda = 0$, or *TD(0)*. Although TD(0) is not optimal for all data sets, it is strictly superior to TD(1), has a trivial implementation (no need for eligibility traces), and does not risk overfitting to our test set.

Anytime Prediction and Speed-Accuracy Trade Offs

Given a static input, an anytime prediction model attempts to obtain the best classification possible as quickly as possible. Anytime prediction can be performed by both serial and cascaded models. Both yield predictions at each time slice, as depicted by the yellow trapezoids in Figures 1b,c, which denote model readout. Critical to anytime prediction is

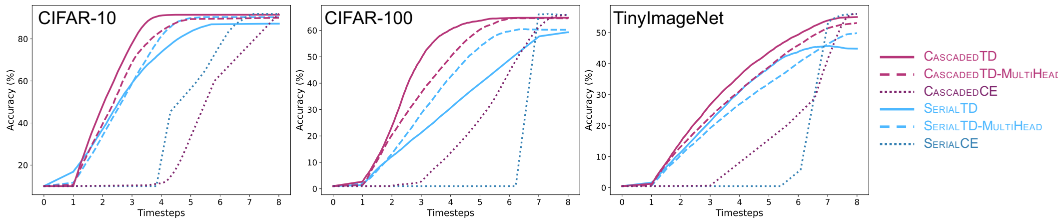

Figure 4: Speed accuracy trade off for three data sets and six models, obtained by varying a stopping threshold and measuring mean latency and mean accuracy. CascadedTD is our parallel anytime prediction model; SerialTD-MultiHead is the state-of-the-art method, SDN [23].

deciding when to terminate processing and initiate a response [6, 23, 46]. Following [23] and [46], we assume that processing terminates when the confidence (probability) for the most likely class rises above threshold θ. For any θ, one can measure the mean stopping time and the mean accuracy for all instances in a test set. By sweeping $\theta \in [0, 1]$ and plotting mean accuracy as a function of mean stopping time, one obtains a *speed-accuracy trade off* curve. Figure 4 shows curves for models we'll describe next.

To evaluate the cascaded model, we compare to a recent state-of-the-art method, the *Shallow-Deep Network (SDN)* [23]. The SDN has the serial architecture depicted in Figure 1b. One critical design decision was whether to have separate read-out heads at each step (MultiHead) or a shared read-out head (SingleHead), i.e., whether weights are separate or shared. From the perspective of the cascaded model, which considers the vertical columns of Figure 1c to be copies of a network unrolled in time, the SingleHead approach is natural. The SDN, as a serial model, chose the MultiHead approach. We tested all four logical combinations of {SerialTD, CascadedTD} × {SingleHead, MultiHead}. We use SerialTD and CascadedTD as shorthand for the SingleHead variants, and append MultiHead to the model name for that version. Additionally, we consider SerialCE and CascadedCE, which are SingleHead variants trained with the standard cross entropy loss that penalizes only asymptotic accuracy and does not explicitly attempt to obtain a speeded response.

Let's step through key observations from Figure 4, which shows speed-accuracy trade offs for the six models on three data sets. First, our canonical cascaded model, CascadedTD, obtains better anytime prediction than SerialTD-MultiHead (i.e., the architecture of SDN). CascadedTD also achieves higher asymptotic accuracy; its accuracy matches that of CascadedCE, a ResNet trained in the standard manner. Thus, cascaded models can exploit parallelism to obtain computational benefits in speeded perception without costs in accuracy.[2] Second, while MultiHead is superior to SingleHeadfor serial models, the reverse is true for cascaded models. This finding is consistent with the cascaded architecture's perspective on anytime prediction as unrolled iterative estimation, rather than, as cast in SDN, as distinct read out heads from different layers of the network. Third, models trained with TD outperform models trained with standard cross-entropy loss. Training for speeded responses reorganizes knowledge in the network so that earlier layers are more effective in classifying instances. We now turn to better understanding what this reorganization entails.

Organization of Knowledge in TD-Trained Cascaded Model

Having examined the response profile of our models over an evaluation set, we now turn to analyzing the response to individual instances. Specifically, we ask about the time course of reaching a classification decision. We define the *selection latency* for an instance to be the minimum number of steps required to reach a confidence threshold on one class and maintain that level going forward, i.e., $\min\{t \mid [\exists j \mid \hat{y}_{t',j} > \theta \;\forall\, t' \geq t]\}$, where $\hat{y}$ is the model output, j is an index over classes, and θ is the threshold. The selection latency does not specify whether or not the chosen class is correct. We picked a threshold $\theta = 0.83$ for CascadedTD such that only $\sim 10\%$ of the test examples failed to reach threshold; results that follow are robust to this selection.

[2] We used $\lambda = 1$ to train SerialTD and SerialTD-MultiHead, as was done for *all* previously proposed serial models. Could SDN and other serial models be improved with $\lambda < 1$? In the Appendix, we show that the serial model with $\lambda = 0$ still does not perform as well as CascadedTD.

Table 1: Spearman rank correlations between three measures of instance prototypicality and selection latency. Larger coefficient indicates faster responses for more prototypical instances.

Measure	Spearman's ρ	
	CascadedCE	CascadedTD
centrality	0.140	0.352
C-score	0.326	0.489
human consistency	0.153	0.142

What determines an instance's selection latency? Figure 2 presents instances that have the lowest and highest latency—labeled 'rapid' and 'slow', respectively. For CascadedTD (Figure 2a), notice the homogeneity of the rapid images: the objects are viewed from a canonical perspective and lie against a solid background with no clutter in the image; in contrast, the slow images are more varied, both in the object's instantiation in the image and the background complexity. Turning to CascadedCE (Figure 2b), instances do not appear to stratify by prototypicality. In the rest of this section, we formalize the notion of prototypicality with three measures and compute the correlation of each measure with selection latency for the cascaded model trained with a TD loss (CascadedTD) and with the standard cross-entropy loss (CascadedCE). Our three measures are as follows.

- *Centrality.* We compute the cosine distance of an instance's embedding (the penultimate layer activation) and the target-class weight vector. The larger this quantity, the better aligned the two vectors are. Because the weight vector will tend to point near the center of class instances, the cosine distance is a measure of instance centrality.
- *C-score.* Jiang et al. [20] describe an instance-based measure of statistical regularity called the C-score. The C-score is an empirical estimate of the probability that a network will generalize correctly to an instance if it is held out from the training set. It reflects statistical regularity in that an instance similar to many other instances in the training set should have a high C-score.
- *Human labeling consistency.* Peterson et al. [37] collected human labels on images. Most images are consistently labeled, but some are ambiguous. The negative entropy of the response distribution indicates inter-human labeling agreement. Presumably consistently labeled instances are more prototypical.

All three measures are available only for the CIFAR-10 training set. Consequently, we ran 10-fold cross validation on the training set, assessing the correlation based on the held out images in each fold. To obtain a granular selection latency, we use the EWS kernel.

Table 1 presents the correlation—Spearman's ρ—between the three prototypicality measures and negative selection latency for CascadedCE and CascadedTD. A positive coefficient indicates shorter latency for prototypical instances. The coefficient is reliably positive ($p < .001$) for each of the three typicality measures and both models. However, CascadedTD obtains reliably higher correlations on two of the three measures than CascadedCE ($p < .001$). They are not significantly different on the consistency measure ($p = .29$). Thus, by these quantitative scores, the TD training procedure leads to better stratification of instances by typicality, in line with the qualitative results presented in Figure 2. Why does TD training distinguish instances based on prototypicality? Intuitively, a prototypical instance shares features with many other class instances. Because these features are frequent in the data set, the TD loss focuses on rapidly classifying instances with those features.

Beyond investigating the time course of fine-grain classification, we also examined coarse-grain classification. Forming twenty superclasses from the 100 fine-grain classes of CIFAR-100, as

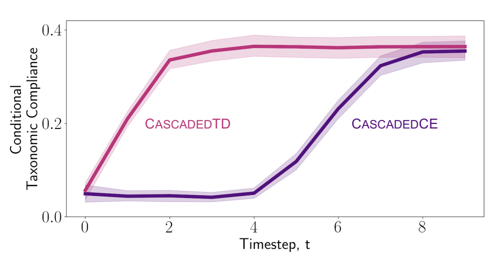

Figure 5: CascadedTD performs coarse-grain classification before fine-train classification, as assessed by a measure of conditional taxonomic compliance [52]. Graphs are based on 5 runs of each model with different random initializations. Shaded error bands indicate ±1 SEM, corrected to remove performance variance due to initial seed [31].

Figure 6: Lossy noise types. From left to right: *Focus*, *Perlin*, *Occlusion*, *Resolution*.

specified in [25], we examined the probability of correct coarse-grain classification conditional on incorrect fine-grain classification. Zamir et al. [52] refer to this probability as *taxonomic compliance*, which reflects information being transmitted about coarse category even when the specific class cannot be determined. As shown in Figure 5, taxonomic compliance rises faster for CascadedTD than for CascadedCE. Whereas chance compliance is .05, CascadedTD achieves a compliance probability of .35 after 2 steps. CascadedCE requires 8 steps to achieve the same performance. TD training pushes instances to the correct semantic neighborhood sooner, even when not to the correct class label. This result further supports the reorganization of knowledge for more robust behavior.

Robustness to Input Noise

In previous simulations, we have assumed the input was static while internal processing took place. Now we consider static inputs with time-varying noise. Figure 6 shows four types of lossy noise we consider on CIFAR-10 images. The noise types are: (1) *Focus*: a 16×16 foveated patch randomly placed within the image, where regions outside of the patch are Gaussian blurred; (2) *Perlin*: gradient noise randomly applied to 40% of image pixels; (3) *Occlusion*: a 16×16 occluding patch randomly placed within the image; (4) *Resolution*: random downsampling by factors of $0\times$, $2\times$, or $4\times$ via average pooling followed by k-nearest upsampling to recover the original dimensionality of 32×32.

For each noise type, CascadedCE and CascadedTD models are trained with the corresponding image transformation type as a data augmentation. Training details can be found in the Appendix. Because the external environment changes more rapidly than any snapshot of the environment can be processed, cascaded models will necessarily integrate signals from multiple snapshots. To determine whether signal integration is beneficial for noise suppression, we compared to a serial model that is allowed to fully process each snapshot, which for the architecture requires $9\times$ as many sequential updates as the cascaded model. We therefore refer to the model as SerialCE×9; it has the same weights as CascadedCE.

Two noise variants are applied to test images: *persistent*, in which a noise sample is drawn independently at each update step, and *transient*, in which the model reaches its asymptotic output on a noise-free input, input is corrupted by noise samples for a variable number of steps, and then the noise-free is presented input until the model returns to its previous asymptotic output. For persistent noise, we assess with asymptotic accuracy; for transient noise, we assess with a measure of *drop in integrated performance* over the course of the episode, which indicates how quickly the model recovers from noise perturbation (smaller is better). Simulation details in the Appendix.

Table 2 indicates that CascadedTD obtains a degree of robustness to persistent and transient noise not matched by the alternative models. Although SerialCE×9 performs a full inference pass on each noise perturbation, the stateful nature of CascadedTD allows it to smooth out noise via slow integration. Although CascadedCE shares the same architecture as CascadedTD, TD training is required to orchestrate the integration of content-specific perceptual information. This experiment indicates that laggy information processing in the

Table 2: Experiments on persistent and transient input noise. Highlight indicates best performance.

	Persistent Noise *Asymptotic Accuracy (%)*			**Transient Noise** *Drop in Integrated Performance*		
Noise	SerialCE×9	CascadedCE	CascadedTD	SerialCE×9	CascadedCE	CascadedTD
Focus	84.27 ± 0.06	83.75 ± 0.10	87.31 ± 0.04	0.62 ± 0.04	0.66 ± 0.05	0.00 ± 0.01
Occlusion	86.26 ± 0.08	82.73 ± 0.09	89.76 ± 0.05	7.70 ± 0.55	8.25 ± 0.72	0.93 ± 0.15
Perlin	85.18 ± 0.03	84.56 ± 0.05	87.67 ± 0.08	0.86 ± 0.06	0.87 ± 0.07	0.00 ± 0.01
Resolution	84.53 ± 0.07	85.40 ± 0.07	88.19 ± 0.10	0.81 ± 0.06	0.53 ± 0.05	0.18 ± 0.02

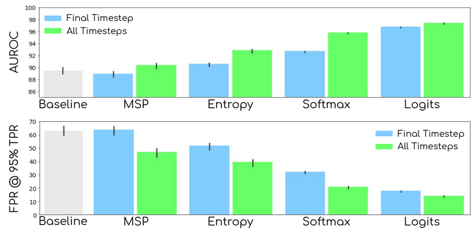

Figure 7: The output of CascadedTD over time provides a signal for significantly improving OOD detection over just using its asymptotic output. Larger AUROC and smaller FPR are better. All output representations benefit from the temporal trajectory. Error bars reflect ± 1 SEM corrected to remove comparison-unrelated variance [31]. Baseline comes directly from the final max softmax prediction.

cascaded model can be advantageous in a noisy environment. In the Appendix, we note that the benefit for CascadedTD applies only to lossy noise, not translations and rotations.

Meta-cognitive Inference

In this section, we consider the hypothesis that temporally intermediate outputs from cascaded networks can provide additional signals to improve performance. We term this *metacognition*, by reference to human abilities to reason about our reasoning processes.

The temporal trace of output from CascadedTD is provided to a separate classifier, MetaCog, which is *discriminatively* trained for OOD detection. MetaCog is a fully connected feedforward net with a 256-unit hidden layer and a sigmoidal output unit for binary prediction: 1 or 0 for in- or out-of-distribution instances, respectively. CIFAR-10's validation set serves as the in-distribution training examples, whereas the validation sets of TinyImageNet, LSUN, and SVHN serve as OOD training examples; see details in Appendix. The CascadedTD output is represented in one of four ways as input to MetaCog: (1) the confidence of the most probable class, known as the *max softmax prediction* (*MSP*), (2) entropy of the class posterior distribution, (3) the class posterior distribution, and (4) the logit representation of the posterior. We investigate whether feeding the output of all time steps to MetaCog leads to improved prediction relative to feeding only the final asymptotic output. Only the latter information is available in a standard feedforward net.

Following [29], we assess OOD performance with *AUROC*, the area under the ROC curve, and *FPR @ 95% TPR*, the false positive rate at 95% true positive rate. A baseline metric is computed directly from the final max softmax predictions of the CascadedTD model, whereas the other metrics are based on the MetaCog model output. Figure 7 indicates that the temporal output trajectory of CascadedTD provides a valuable signal for OOD detection. Our goal here was not to propose a method for OOD detection, but merely to demonstrate that in principle, there is information about the input that is conveyed by the cascaded model's dynamics but that is not available in a traditional classifier's output.

Discussion

We investigated a neglected biologically-motivated architecture in which transmission delays are the bottleneck in neural information processing, not the number of neurons that can update in parallel. We proposed a temporal-difference (TD) loss that yields improved speed-accuracy trade offs. We showed that this model beats the state-of-the-art anytime prediction method, partly because of the TD loss and partly because of the model dynamics. The cascaded model has many distinctive properties, including: it classifies prototypical instances more rapidly than outliers; it performs coarse-to-fine semantic processing in which general semantic categories are rapidly inferred even if specific class labels are not; it is able to moderate time-varying input noise; and the temporal trace of the model's output provides an additional signal that can be exploited to improve information processing beyond that provided by the asymptotic model output. Of course, these interesting properties come at a computational cost when parallel hardware is simulated on existing compute infrastructure. We see three directions in which cascaded nets have particular potential.

- For neuroscientists using deep nets as a model of human vision, cascaded nets are a better approximation to the dynamics of the neural hardware. The properties we investigate—neurons operate in parallel, neurons are stateful, and neurons are slow to transmit information—seem likely to have a critical impact on the nature of cortical computing. As one simple illustration, cortical feedback processes are often posited to be critical for explaining difference in processing efficiency of visual stimuli [e.g., 22, 41]. We have shown that these difference might be partly explained by feedforward cascaded dynamics.

- For hardware researchers, cascaded networks are a possible direction for the future design of AI hardware. It is a direction quite unlike modern GPUs and TPUs, one that exploits massively parallel albeit slow and possibly noisy information processing. Our success in showing strong performance from cascaded models, as well as a training procedure to obtain quick and accurate responses, should encourage researchers in this direction.
- For AI research in anytime prediction, we've shown that existing models can be improved with a TD(λ) loss; all past research has adopted $\lambda = 1$, which we show to be inferior to $\lambda < 1$. For researchers who care little about cascaded models per se, cascaded models offer an intriguing method to train serial feedforward models. One can take a serial feedforward model, turn it into a cascaded model for training with TD methods, and then run it in serial mode. We've shown that TD training can improve asymptotic model accuracy while still providing anytime predictions due to inductive biases it imposes on the organization of representations.

References

[1] William Bialek and Fred Rieke. Reliability and information transmission in spiking neurons. *Trends in Neurosciences*, 15(11):428–434, 1992. ISSN 0166-2236.

[2] Tolga Bolukbasi, Joseph Wang, Ofer Dekel, and Venkatesh Saligrama. Adaptive neural networks for efficient inference. In *International Conference on Machine Learning*, pages 527–536. PMLR, 2017.

[3] Adrian Bulat and Georgios Tzimiropoulos. How far are we from solving the 2D & 3D face alignment problem? In *Proceedings of the IEEE International Conference on Computer Vision*, pages 1021–1030, 2017.

[4] Adrian Bulat, Jean Kossaifi, Georgios Tzimiropoulos, and Maja Pantic. Toward fast and accurate human pose estimation via soft-gated skip connections. *arXiv preprint arXiv:2002.11098*, 2020.

[5] Joao Carreira, Viorica Patraucean, Laurent Mazare, Andrew Zisserman, and Simon Osindero. Massively parallel video networks. In *Proceedings of the European Conference on Computer Vision (ECCV)*, pages 649–666, 2018.

[6] Xinshi Chen, Hanjun Dai, Yu Li, Xin Gao, and Le Song. Learning to stop while learning to predict. In Hal Daumé III and Aarti Singh, editors, *Proceedings of the 37th International Conference on Machine Learning*, volume 119 of *Proceedings of Machine Learning Research*, pages 1520–1530. PMLR, 13–18 Jul 2020.

[7] Jia Deng, Wei Dong, Richard Socher, Li-Jia Li, Kai Li, and Li Fei-Fei. Imagenet: A large-scale hierarchical image database. In *2009 IEEE conference on computer vision and pattern recognition*, pages 248–255. Ieee, 2009.

[8] Maha Elbayad, Jiatao Gu, Edouard Grave, and Michael Auli. Depth-adaptive transformer. In *International Conference on Learning Representations*, 2020. URL `https://openreview.net/forum?id=SJg7KhVKPH`.

[9] Daniel J Felleman and David C Van Essen. Distributed hierarchical processing in the primate cerebral cortex. In *Cereb cortex*. Citeseer, 1991.

[10] Volker Fischer, Jan Köhler, and Thomas Pfeil. The streaming rollout of deep networks-towards fully model-parallel execution. In *Advances in Neural Information Processing Systems*, pages 4039–4050, 2018.

[11] Kunihiko Fukushima. Neocognitron: A self-organizing neural network model for a mechanism of pattern recognition unaffected by shift in position. *Biological Cybernetics*, 36:193–202, 1980.

[12] Alex Graves. Adaptive computation time for recurrent neural networks. *CoRR*, abs/1603.08983, 2016.

[13] Kaiming He, Xiangyu Zhang, Shaoqing Ren, and Jian Sun. Deep residual learning for image recognition. In *Proceedings of the IEEE conference on computer vision and pattern recognition*, pages 770–778, 2016.

[14] Hanzhang Hu, Debadeepta Dey, Martial Hebert, and J. Andrew Bagnell. Anytime neural network: a versatile trade-off between computation and accuracy, 2018. URL `https://openreview.net/forum?id=SJa1Nk10b`.

[15] Hanzhang Hu, Debadeepta Dey, Martial Hebert, and J Andrew Bagnell. Learning anytime predictions in neural networks via adaptive loss balancing. In *Proceedings of the AAAI Conference on Artificial Intelligence*, volume 33, pages 3812–3821, 2019.

[16] Gao Huang, Danlu Chen, Tianhong Li, Felix Wu, Laurens van der Maaten, and Kilian Q Weinberger. Multi-scale dense networks for resource efficient image classification. *arXiv preprint arXiv:1703.09844*, 2017.

[17] Gao Huang, Zhuang Liu, Laurens Van Der Maaten, and Kilian Q Weinberger. Densely connected convolutional networks. In *Proceedings of the IEEE conference on computer vision and pattern recognition*, pages 4700–4708, 2017.

[18] Gao Huang, Danlu Chen, Tianhong Li, Felix Wu, Laurens van der Maaten, and Kilian Weinberger. Multi-scale dense networks for resource efficient image classification. In *International Conference on Learning Representations*, 2018. URL `https://openreview.net/forum?id=Hk2aImxAb`.

[19] Michael Iuzzolino, Yoram Singer, and Michael C Mozer. Convolutional bipartite attractor networks. *arXiv preprint arXiv:1906.03504*, 2019.

[20] Ziheng Jiang, Chiyuan Zhang, Kunal Talwar, and Michael C Mozer. Characterizing structural regularities of labeled data in overparameterized models. In *Proceedings of the International Conference on Machine Learning*, 2021.

[21] Matt Jones, Sachiko Kinoshita, and Michael C Mozer. Optimal response initiation: Why recent experience matters. In D. Koller, D. Schuurmans, Y. Bengio, and L. Bottou, editors, *Advances in Neural Information Processing Systems*, volume 21. Curran Associates, Inc., 2009.

[22] Kohitij Kar, Jonas Kubilius, Kailyn Schmidt, Elias B. Issa, and James J. DiCarlo. Evidence that recurrent circuits are critical to the ventral stream's execution of core object recognition behavior. *Nature Neuroscience*, 04/2019 2019.

[23] Yigitcan Kaya, Sanghyun Hong, and Tudor Dumitras. Shallow-deep networks: Understanding and mitigating network overthinking. In *International Conference on Machine Learning*, pages 3301–3310. PMLR, 2019.

[24] Nikolaus Kriegeskorte. Deep neural networks: A new framework for modeling biological vision and brain information processing. *Annual Review of Vision Science*, 1(1):417–446, 2015.

[25] Alex Krizhevsky. Learning multiple layers of features from tiny images. Technical report, Computer Science, University of Toronto, 2009.

[26] Omkar Kumbhar, Elena Sizikova, Najib J. Majaj, and Denis G. Pelli. Anytime prediction as a model of human reaction time. *CoRR*, abs/2011.12859, 2020. URL `https://arxiv.org/abs/2011.12859`.

[27] Gustav Larsson, Michael Maire, and Gregory Shakhnarovich. Fractalnet: Ultra-deep neural networks without residuals. In *International Conference on Learning Representations*, 2017.

[28] Hankook Lee and Jinwoo Shin. Anytime neural prediction via slicing networks vertically. *arXiv preprint arXiv:1807.02609*, 2018.

[29] Shiyu Liang, Yixuan Li, and Rayadurgam Srikant. Enhancing the reliability of out-of-distribution image detection in neural networks. *arXiv preprint arXiv:1706.02690*, 2017.

[30] Enrique S Marquez, Jonathon S Hare, and Mahesan Niranjan. Deep cascade learning. *IEEE transactions on neural networks and learning systems*, 29(11):5475–5485, 2018.

[31] Michael EJ Masson and Geoffrey R Loftus. Using confidence intervals for graphically based data interpretation. *Canadian Journal of Experimental Psychology/Revue canadienne de psychologie expérimentale*, 57(3):203, 2003.

[32] James L McClelland. On the time relations of mental processes: an examination of systems of processes in cascade. *Psychological review*, 86(4):287, 1979.

[33] Warren S. McCulloch and Walter Pitts. A logical calculus of the ideas immanent in nervous activity. *Bulletin of Mathematical Biophysics*, 5(4):115–133, 1943.

[34] Lane McIntosh, Niru Maheswaranathan, David Sussillo, and Jonathon Shlens. Recurrent segmentation for variable computational budgets. In *Proceedings of the IEEE Conference on Computer Vision and Pattern Recognition Workshops*, pages 1648–1657, 2018.

[35] Yuval Netzer, Tao Wang, Adam Coates, Alessandro Bissacco, Bo Wu, and Andrew Y. Ng. Reading digits in natural images with unsupervised feature learning. In *NIPS Workshop on Deep Learning and Unsupervised Feature Learning 2011*, 2011. URL `http://ufldl.stanford.edu/housenumbers/nips2011_housenumbers.pdf`.

[36] Alejandro Newell, Kaiyu Yang, and Jia Deng. Stacked hourglass networks for human pose estimation. In *European conference on computer vision*, pages 483–499. Springer, 2016.

[37] Joshua C Peterson, Ruairidh M Battleday, Thomas L Griffiths, and Olga Russakovsky. Human uncertainty makes classification more robust. In *Proceedings of the IEEE International Conference on Computer Vision*, pages 9617–9626, 2019.

[38] R. Ratcliff and G. McKoon. The diffusion decision model: theory and data for two-choice decision tasks. *Neural Computation*, 20(4):873—922, 2008.

[39] Olaf Ronneberger, Philipp Fischer, and Thomas Brox. U-net: Convolutional networks for biomedical image segmentation. In *International Conference on Medical image computing and computer-assisted intervention*, pages 234–241. Springer, 2015.

[40] Simone Scardapane, Michele Scarpiniti, Enzo Baccarelli, and Aurelio Uncini. Why should we add early exits to neural networks? *Cognitive Computation*, 12(5):954–966, 2020.

[41] Courtney J. Spoerer, Patrick McClure, and Nikolaus Kriegeskorte. Recurrent convolutional neural networks: A better model of biological object recognition. *Frontiers in Psychology*, 8:1551, 2017. URL `https://www.frontiersin.org/article/10.3389/fpsyg.2017.01551`.

[42] Courtney J Spoerer, Tim C Kietzmann, Johannes Mehrer, Ian Charest, and Nikolaus Kriegeskorte. Recurrent neural networks can explain flexible trading of speed and accuracy in biological vision. *bioRxiv*, 2020. URL `https://www.biorxiv.org/content/early/2020/08/21/677237`.

[43] Rupesh Kumar Srivastava, Klaus Greff, and Jürgen Schmidhuber. Highway networks. *arXiv preprint arXiv:1505.00387*, 2015.

[44] Richard S Sutton. Learning to predict by the methods of temporal differences. *Machine learning*, 3(1):9–44, 1988.

[45] Richard S Sutton and Andrew G Barto. *Reinforcement learning: An introduction*. MIT press, 2018.

[46] Surat Teerapittayanon, Bradley McDanel, and Hsiang-Tsung Kung. Branchynet: Fast inference via early exiting from deep neural networks. In *2016 23rd International Conference on Pattern Recognition (ICPR)*, pages 2464–2469. IEEE, 2016.

[47] Ashish Vaswani, Noam Shazeer, Niki Parmar, Jakob Uszkoreit, Llion Jones, Aidan N Gomez, Ł ukasz Kaiser, and Illia Polosukhin. Attention is all you need. In I. Guyon, U. V. Luxburg, S. Bengio, H. Wallach, R. Fergus, S. Vishwanathan, and R. Garnett, editors, *Advances in Neural Information Processing Systems*, volume 30. Curran Associates, Inc., 2017.

[48] Xin Wang, Yujia Luo, Daniel Crankshaw, Alexey Tumanov, Fisher Yu, and Joseph E Gonzalez. Idk cascades: Fast deep learning by learning not to overthink. *arXiv preprint arXiv:1706.00885*, 2017.

[49] Le Yang, Yizeng Han, Xi Chen, Shiji Song, Jifeng Dai, and Gao Huang. Resolution adaptive networks for efficient inference. In *Proceedings of the IEEE/CVF Conference on Computer Vision and Pattern Recognition*, pages 2369–2378, 2020.

[50] Fisher Yu, Ari Seff, Yinda Zhang, Shuran Song, Thomas Funkhouser, and Jianxiong Xiao. Lsun: Construction of a large-scale image dataset using deep learning with humans in the loop. *arXiv preprint arXiv:1506.03365*, 2015.

[51] Sergey Zagoruyko and Nikos Komodakis. Wide residual networks. *arXiv preprint arXiv:1605.07146*, 2016.

[52] Amir R Zamir, Te-Lin Wu, Lin Sun, William B Shen, Bertram E Shi, Jitendra Malik, and Silvio Savarese. Feedback networks. In *Proceedings of the IEEE Conference on Computer Vision and Pattern Recognition*, pages 1308–1317, 2017.

[53] Shlomo Zilberstein. Using anytime algorithms in intelligent systems. *AI magazine*, 17 (3):73–73, 1996.

A Experiment Details

A.1 CascadedCE and CascadedTD Experiment Details

For all cascaded and serial models, we used a ResNet-18 for CIFAR-10, CIFAR-100, and TinyImageNet datasets. We experimented with deeper nets, up to ResNet-52, but found no differences in model behavior. The models were trained using data parallelism over 8 GPUs (see §A.6 for infrastructure details), with the model on each GPU using a batch size of 128. SGD with Nesterov momentum, an initial learning rate of 0.1, weight decay of 0.005, and momentum of 0.9 was used to optimize a softmax cross-entropy loss for SerialCE/CascadedCE and a temporal difference cross-entropy loss for SerialTD/CascadedTD. All models were trained for 120 epochs and the learning rate was decayed with a multiplicative factor of 0.2 every 30 epochs.

The training datasets were split (class-balanced) as 90-10 train-validation, where the validation splits were held out for downstream tasks, such as training MetaCog models (see Appendix B). For CascadedTD, the batch normalization layer must be augmented such that running means and variances are tracked independently for each timestep. At run-time, if the maximum number of timesteps used during training is exceeded, as occurs with the EWS kernel, the final timestep statistics of the batch normalization layers are used for all subsequent timesteps. Furthermore, we observed that the offset parameter of the affine transformation of the batch normalization on identity mappings explodes during training; consequently, we do not use batch normalization on the identity mapping in the cascaded nor serial models.

A.2 Temporal Difference Loss

A.2.1 Incremental TD Formulation

TD(λ) amounts to training at each time step t with a target, y_t^λ, that is an exponentially decaying trace of future outputs, anchored beyond some asymptotic time T to the true target, y. Denoting the network output at step $t \in \{1, \ldots, T\}$ as $\hat{y}_t$, the trace is:

$$
\begin{aligned}
y_t^\lambda &= (1-\lambda) \sum_{n=1}^{\infty} \lambda^{n-1} \bar{y}_{t+n} \\
&\qquad \text{with} \;\; \bar{y}_{t+n} = \begin{cases} \hat{y}_{t+n} & \text{if } t+n \le T \\ y & \text{otherwise} \end{cases} \\
&= (1-\lambda) \sum_{n=1}^{T-t} \lambda^{n-1} \hat{y}_{t+n} + \lambda^{T-t} y.
\end{aligned}
$$

We train with cross entropy loss over all time steps. For a single example, the loss is

$$\mathcal{L} = -\sum_{t,i} y_{ti}^\lambda \ln \bar{y}_{ti}.$$

The derivative of this loss with respect to the network parameters w can be expressed in terms of the derivative with respect to the logits:

$$\nabla_w \mathcal{L} = -\sum_{t,i} (y_{ti}^\lambda - \bar{y}_{ti}) \nabla_w z_{ti},$$

where z_{ti} is the logit of class i at step t. The temporal difference method provides a means of computing this gradient incrementally, such that at each step t, an update can be computed based on only the difference of model outputs at t and $t+1$:

$$\nabla_w^{\text{TD}} \mathcal{L} = -\sum_{t,i} (\bar{y}_{t+1,i} - \bar{y}_{ti}) e_{ti},$$

where e_{ti} is an *eligibility trace*, defined as:

$$e_{ti} = \begin{cases} \mathbf{0} & \text{if } t = 0 \\ \lambda e_{t-1,i} + \nabla_w z_{ti} & \text{if } t \ge 1 \end{cases}$$

Table A.1: Asymptotic accuracy for CascadedTD models for various λ, as well as CascadedCE. Green font indicates best performance across TD(λ) and CascadedCE models for a given dataset. Highlight indicates best performing TD(λ) across λ's for a given dataset.

	Cascaded Model Variant					
Dataset	**TD(0)**	**TD(0.25)**	**TD(0.5)**	**TD(0.83)**	**TD(1)**	**CE**
CIFAR-10	91.22 ± 0.18	91.65 ± 0.08	91.45 ± 0.16	90.98 ± 0.21	88.75 ± 0.42	91.91 ± 0.08
CIFAR-100	67.48 ± 0.14	67.35 ± 0.20	67.00 ± 0.18	65.06 ± 0.11	63.20 ± 0.14	65.56 ± 0.06
TinyImageNet	50.74 ± 0.11	52.03 ± 0.07	52.25 ± 0.07	51.39 ± 0.13	49.86 ± 0.15	52.46 ± 0.06

The incremental formulation of TD via $\nabla_w^{\text{TD}}\mathcal{L}$ is valuable when gradients and/or weight updates must be computed on line rather than presenting an entire sequence before computing the loss, e.g., in the situation where the network runs for many steps and truncated BPTT is required. In our experiments, we use the summed gradient, $\nabla_w\mathcal{L}$, computed by PyTorch from the full T step sequence and our exponentially weighted target, y_t^λ.

A.2.2 TD(λ) Sweep

Table A.1 shows the tabulated results for asymptotic accuracy of CascadedTD swept over λ values on CIFAR-10, CIFAR-100, and TinyImageNet, as well as CascadedCE. Note, 5 trials per λ were trained for each dataset.

A.3 Data Augmentation

When training all models on CIFAR-10 and CIFAR-100, for each batch the 32×32 images are padded with 4 pixels to each border (via reflection padding), resulting in a 40×40 image. A random 32×32 crop is taken, the image is randomly flipped horizontally, and standard normalized using the training set statistics is applied. Finally, a random 8×8 block cut is taken such that the cropped pixels are set to 0. Images at run-time are only standard normalized using training set statistics - no other augmentation is applied with the exception of the persistent and noise robustness experiments. The same process is followed for TinyImageNet with the following exceptions: (1) the 64×64 images are padded to 86×86 with reflection padding, random cropped back to 64×64, randomly flipped horizontally, then standard normalized, and (2) no 8×8 block cutting is applied.

A.4 Noise Experiments

The four noise perturbations studied in the main article are lossy. Here we consider two additional noise sources that are roughly information preserving: *Translation*: random shifts ± 8 pixels in (x, y) on a reflection-padded image; *Rotation*: random rotations $\pm 60°$ on a reflection padded image.

SerialCE×9 is best on information preserving transformations such as *Translation* and *Rotation* because it is performing a full inference pass on the input whereas the cascaded models are performing a single update step.

While both CascadedTD and CascadedCE smooth responses over frames, CascadedTD performs better, indicating that beyond smoothing, TD training orchestrates the integration of image-specific perceptual information. This integration matters more for lossy transformations, where information integration is essential.

The training details are the same as previous simulations, except that we discard the 8×8 block data augmentation in order to avoid biasing the models toward the *Occlusion* noise transformation. We evaluate the cascaded models with the OSD kernel to allow for a comparison of cascaded models with SerialCE×9.

In the persistent-noise experiment, five trials are run per image in the test set. In the transient-noise experiment, we present the noise-free input for 10 time steps (sufficient for the cascaded models to reach asymptote), apply one of the six noise transforms for N time steps, and then present the noise-free input for another 10 steps, allowing the model to return to its asymptotic state. We run five trials per condition for each $N \in \{1, 2, 3, 4, 5, 6\}$ and each image in the test set. Performance is evaluated as the drop-in-integrated-performance,

Figure A.1: Noise types. From left to right, top to bottom: *Focus*, *Perlin*, *Translation*, *Occlusion*, *Resolution*, *Rotation*.

Table A.2: Persistent-noise experiment. Highlight indicates best asymptotic performance for a given noise type.

Persistent	Asymptotic Model Performance		
Noise	SerialCEx9	CascadedCE	CascadedTD
Focus	84.27 ± 0.06	83.75 ± 0.10	87.31 ± 0.04
Occlusion	86.26 ± 0.08	82.73 ± 0.09	89.76 ± 0.05
Perlin	85.18 ± 0.03	84.56 ± 0.05	87.67 ± 0.08
Resolution	84.53 ± 0.07	85.40 ± 0.07	88.19 ± 0.10
Rotation	89.11 ± 0.04	73.79 ± 0.10	87.51 ± 0.03
Translation	87.55 ± 0.12	76.72 ± 0.09	83.42 ± 0.14

Table A.3: Transient-noise experiment. Highlight indicates lowest DIP for a given noise type.

Transient	Drop in Integrated Performance (DIP)		
Noise	SerialCEx9	CascadedCE	CascadedTD
Focus	0.62 ± 0.04	0.66 ± 0.05	0.00 ± 0.01
Occlusion	7.70 ± 0.55	8.25 ± 0.72	0.93 ± 0.15
Perlin	0.86 ± 0.06	0.87 ± 0.07	0.00 ± 0.01
Resolution	0.81 ± 0.06	0.53 ± 0.05	0.18 ± 0.02
Rotation	0.24 ± 0.02	4.12 ± 0.29	0.00 ± 0.01
Translation	0.72 ± 0.05	4.17 ± 0.37	1.53 ± 0.14

DIP $= \hat{y}_T - \mathbb{E}_{t\in\{B,\ldots,T\}}[\hat{y}_t]$, where T is the total time steps in the simulation, B is the onset time of the noise transformations, and $\hat{y}_t$ is the model's target-class confidence at time step t. DIP indicates how quickly a model can recover from noise perturbations.

A.5 Additional Temporal Dynamics Results

A.5.1 Deadline-based stopping criterion

In the main paper, we show speed-accuracy trade offs for models based on a stopping criterion that terminates processing when a *confidence threshold* is reached for one output class. In Figure A.2, we examine an alternative stopping criterion that is based on a *temporal deadline*, i.e., after a certain number of update iterations. When the speed-accuracy curves for the two stopping criteria are directly compared, the confidence-threshold procedure is superior for all models. For this reason, we report the confidence-threshold procedure in the main paper. However, the confidence-threshold procedure does not allow us to readily compute error bars across model replications because the mean stopping time is slightly different for each

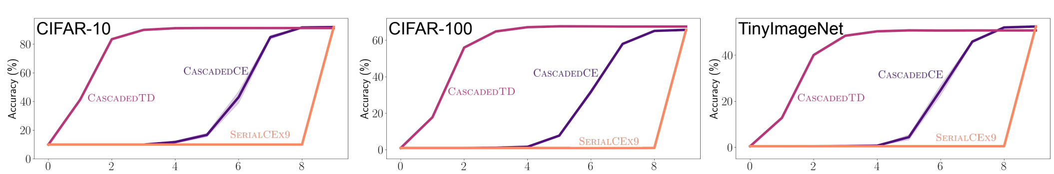

Figure A.2: Speed accuracy trade off for CIFAR-10, CIFAR-100, and TinyImageNet. Here we show the dynamics for a temporal-deadline stopping criterion, whereas Figures 4 and A.3 show speed accuracy trade offs obtained by a confidence threshold-based criterion. Accuracy assuming a particular stopping time is computed for each daedline. Note, SerialCE×9 produces an output only after only all updates. Confidence intervals across model replications are shown by the shaded regions, which are difficult to see because the uncertainty is small.

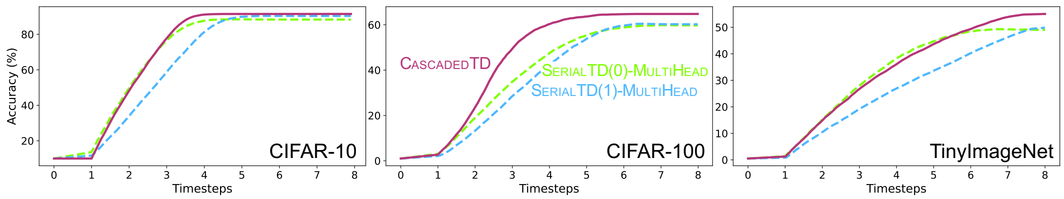

Figure A.3: Comparison of CascadedTD, SerialTD(1)-MultiHead (Shallow-Deep Nets), and SerialTD(0)-MultiHead. Shallow-Deep Nets can be improved using TD(0), but the speed-accuracy trade off is still significantly worse on CIFAR-100, and asymptotic accuracy is lower than that of CascadedTD.

replication. In Figure A.2, we show confidence intervals at the various stopping times using shaded regions. (The regions are very small and are difficult to see.) The main reason for presenting these curves is to convince readers of the reliability of the speed-accuracy curves.

A.5.2 Serial models trained with TD

In the main paper, we compare cascaded models to Shallow-Deep Networks, a serial model with multi-headed outputs trained with TD(1). Just as training with $\lambda < 1$ improves performance of CascadedTD, one might hope to observe a similar benefit for serial models such as Shallow-Deep Networks. Figure A.3 shows that indeed training with TD(0) is superior to training with TD(1) for SDNs, labeled in the graph as SerialTD-MultiHead. The serial model's performance improves significantly, nearly to the level of CascadedTD, for two data sets, but for the third, CascadedTD still has a considerable advantage over the serial model, whether trained with $\lambda = 0$ or $\lambda = 1$.

A.5.3 Qualitative performance of TD trained models on CIFAR-10

Figure A.4 shows CIFAR-10 instances with low and high *selection latency* for both CascadedTD and CascadedCE models. As with CIFAR-100, the qualitative differences between low and high selection latency for CascadedTD are stark, with low selection latency instances being more representative of prototypical instances of the given class (e.g., boats on blue water; horses in fields), whereas high selection latency instances are less typical (e.g., boats on green grass; horses in snow). In contrast, the strong delineation between low and high selection latency groups is not observed for CascadedCE, supporting the claim that TD training allows the model to more rapidly respond to prototypical exemplars.

Figure A.4: CIFAR-10 examples of low and high selection latency resulting from CascadedTD (*left*) and CascadedCE (*right*).

A.6 Computing Infrastructure

We used 8x NVIDIA Telsa V100's on Google Cloud Platform (GCP) for training all CascadedCE and CascadedTD models; a single V100 was used for all evaluations, and to train MetaCog models. All models were implemented in PyTorch v1.5.0, using Python 3.7.7 operating on Ubuntu 18.04.

Table A.4: Average runtime for training CascadedCE and CascadedTD over CIFAR-10, CIFAR-100, and TinyImageNet.

Dataset	Model	Average Runtime (hours)
CIFAR-10	CascadedCE	1.48 ± 0.002
	CascadedTD	1.81 ± 0.001
CIFAR-100	CascadedCE	1.48 ± 0.001
	CascadedTD	1.83 ± 0.001
TinyImageNet	CascadedCE	1.45 ± 0.035
	CascadedTD	1.97 ± 0.020

A.7 Average Runtime and Reproducibility

Table A.4 shows average run times (in hours) for CascadedCEand CascadedTD. Variability in run time, expressed as ±1 SEM, is also shown. Reproducibility was ensured in the data pipeline and model training by seeding Random, Numpy, and PyTorch packages, as well as flagging deterministic cudnn via PyTorch API. When sweeping over λ for a given model and dataset, 5 replications were trained to obtain reliability estimates; a fixed set of 5 seeds was for all models to ensure matched initial conditions across models. The average runtime for training MetaCog models on a single V100 GPU requires less than 3 minutes. When training multiple trials for a given MetaCogmodel, all models are initialized with the same weights, and 42 was used to seed all packages as detailed above.

B Meta-cognitive Experiment Details

For all meta-cognitive experiments, training data is generated from the EWS kernel applied to CascadedTD(0).

B.1 OOD Detection Dataset Details

CIFAR-10 serves as the in-distribution dataset, which contains 5,000 validation and 10,000 test set instances. The 5,000 validation instances, which we use as the in-distribution training set for OOD, were derived from a 90-10 train-validation split of the original 50,000 training instances used for training the CascadedTD model. The OOD datasets are as follows:

TinyImagenet The Tiny ImageNet (TinyImageNet) is a 200-class subset of ImageNet [7] and it contains 10,000 validation and 10,000 test instances. Following the methods of [29] we introduce two variations: 1) *resize*; the image is downsampled to 32×32, and 2) *crop*; a random 32×32 crop is taken from the image.

LSUN The Large-scale Scene UNderstanding (LSUN) [50] consists of 10 scenes categories, such as classroom, restaurant, bedroom, etc. It contains 10,000 validation and 10,000 test instances, and similar to TinyImageNet, we use the *resize* and *crop* variations.

SVHN The Street View House Numbers (SVHN) [35] dataset is obtained from house numbers in Google Street View images. It consists of 73,257 validation and 26,032 test set images.

B.2 OOD Detection Training Details

The MetaCog model is trained for 300 epochs with batch sizes of 256. We used Adam with an initial learning rate of 0.001 and weight decay of 0.0005 to optimize a binary cross entropy loss. Dropout with keep probability 0.5 was used for regularization. Numerical values corresponding to Figure 7 are tabulated in Table B.5 with reported SEM corrected to remove random variance [31].

The OOD examples from TinyImageNet and LSUN have crop and resize variations [29] to make them match CIFAR10 images in dimensions. MetaCog is trained per (in-, out-of-distribution) dataset pairing—e.g., (CIFAR-10, SVHN)—and input representation type (discussed below). The respective test set is used for evaluation.

Table B.5: CIFAR-10 (in-distribution) vs. Aggregate OOD dataset quantitative measures corresponding to Figure 7. Each representation may include all time step outputs, t_{all}, or only the final output, t_{final}.

OOD Representation	AUROC	FPR @ 95% TPR
CascadedTD [MSP]	89.5 ± 0.5	63.0 ± 3.5
MetaCog t_{final} [MSP]	88.8 ± 0.5	63.0 ± 3.1
MetaCog t_{all} [MSP]	90.2 ± 0.5	46.4 ± 3.1
MetaCog t_{final} [Entropy]	90.5 ± 0.3	51.2 ± 2.5
MetaCog t_{all} [Entropy]	92.7 ± 0.3	38.9 ± 2.5
MetaCog t_{final} [Softmax]	92.6 ± 0.1	31.7 ± 0.7
MetaCog t_{all} [Softmax]	95.7 ± 0.1	20.5 ± 0.7
MetaCog t_{final} [Logits]	96.7 ± 0.1	17.5 ± 0.4
MetaCog t_{all} [Logits]	97.3 ± 0.1	13.7 ± 0.4

B.3 Response Initiation

We explored a third stopping criterion, in addition to the confidence-threshold and temporal-deadline criteria. The third criterion was based on a meta-cognitive model that observes the output *sequence* from cascaded-model updates and uses this sequence to determine when to stop. To handle sequences, this MetaCog model was an RNN, specifically a GRU, trained with a logistic output unit that produced a binary stop/don't-stop decision. In contrast to the confidence-threshold criterion, which is based solely on the network output at step t, MetaCog in principle uses steps $0 - t$ to make its decision. It produces a continuous output in [0,1], and by stopping when the output rises above a threshold, we can map out a speed-accuracy trajectory analogous to that obtained with the confidence-threshold criterion.

MetaCog is trained for 300 epochs with a batch size of 256. We used Adam with an initial learning rate of 0.0001 and weight decay of 0.0001 to optimize a binary cross entropy loss. The supervised target is 1.0 at step t if the output with highest probability at t remains unchanged for all subsequent steps, or 0.0 otherwise. Essentially, the model is trained to predict when additional compute will change its decision. To obtain a finer granularity on time steps, we trained and evaluated MetaCog with the EWS kernel.

We trained MetaCog to predict when to stop for both CascadedCE and CascadedTD. MetaCog is trained on the 4,500 instances of the CIFAR-10 validation set that have been processed by the cascaded model, yielding a training set of dimension $4,500 \times 70 \times 10$, where there are 70 timesteps and 10 logit values. We generate our evaluation set from the same method above using the CascadedCE model on the 10,000 instance test set.

Figure B.1 shows the response initiation results comparing CascadedTD (left panel) and CascadedCE (right panel) with stopping criterion using MetaCog versus a temporal deadline. The MetaCog criterion yields significant improvements to response initiation for both models. This finding lends support to the notion that there is a signal in the model output over time as information trickles through the cascaded layers. Essentially, MetaCog can interpret the temporal evolution of cascaded model outputs to improve its speed-accuracy trade off.

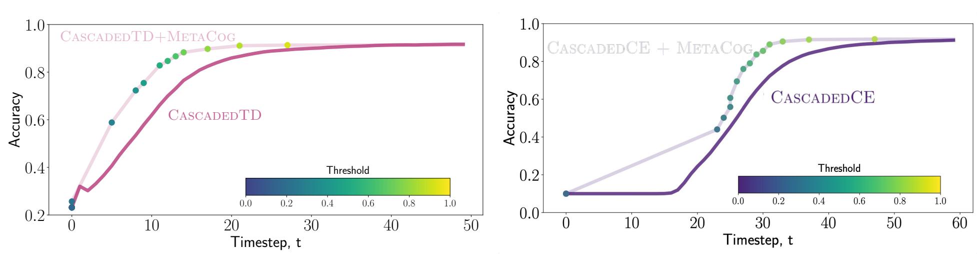

CascadedTD CascadedCE

Figure B.1: Response initiation results comparing two stopping criteria for CascadedTD (left panel) and CascadedCE (right panel). The solid line represents a temporal-deadline stopping criterion. The fainter dotted line uses MetaCog to determine when to stop based on an output threshold.